Refinements to Calandria Tube – Liquid Injection Nozzle (CT-LIN) Contact Assessments

P.J. Sedran

Fuel Channel Consultant – RESD Inc.

ABSTRACT

In recent years, the issue of CT-LIN contact, which first gained attention in 1989, has been addressed through CT-LIN gap measurements, followed by analytical predictions of time-to-contact. CT-LIN time-to-contact predictions have been preformed independently by CPUS Limited for Point Lepreau and Gentilly-2 and by AECL Sheridan Park (now Candu Energy Inc.) for Bruce Power and Gentilly-2. Both companies used the CDEPTH code in combination with CT-LIN gap measurements.

Subsequent to the assessments for Point Lepreau and Gentilly-2, a recommended approach for future assessments was presented at the 2008 CANDU maintenance conference. Since that time, a number of refinements to the overall strategy for predicting CT-LIN time-to-contact have been developed and are outlined in this paper. The refinements include:

1. The use of ultrasonic LIN elevation measurements to confirm LIN creep sag behaviour
2. The development of a non-linear empirical CT Creep Sag Model
3. The development of a rationale for discrepancies observed in repeated optical CT-LIN gap measurements and a discussion of alternative CT-LIN gap measurements

With these refinements, more accurate CT-LIN time-to-contact predictions can be obtained.

For stations that plan to refurbish by 210,000 EFPH, the improvement in time-to-contact predictions resulting from the fore mentioned refinements will not be of any real benefit.. However, for stations that are planning life extensions in order to operate beyond 210,000 EFPH, CT-LIN contact will be an issue. For these stations, improvements in CT-LIN contact time predictions would be beneficial.

This paper presents a summary of the proposed refinements and demonstrates how they would impact CT-LIN time-to-contact predictions.

1. INTRODUCTION

The issue of CT-LIN contact, which first gained attention in 1989, has long been recognized as a life-limiting factor for the CTs. In recent assessments, CT-LIN time–to-contact predictions indicate a significant risk of contact should the reactor operate beyond 210 kEFPH.

In reactors that have been refurbished, (Bruce Units 1 and 2, Point Lepreau, and Wolsong Unit 1), or are planning refurbishment by 210 kEFPH, CT-LIN contact will not be an issue for many years. However, for stations that are planning life extensions in order to operate beyond 210,000 EFPH, CT-LIN contact will be an issue because of potential fretting damage to the CT. For these stations, which would benefit from improvements in time-to-contact prediction accuracy, (Bruce 3 -8 and Darlington) a number of refinements to the overall strategy for predicting CT-LIN time-to-contact have been developed and are outlined in this paper. The refinements include:

1. The use of ultrasonic LIN elevation measurements to confirm LIN creep sag behaviour
2. The development of a non-linear empirical CT Creep Sag Model
3. The development of a rationale for discrepancies observed in repeated optical CT-LIN gap measurements and a discussion of alternative CT-LIN gap measurements

Section 2 contains a summary of the CT-LIN contact work performed to date.

Section 3 provides details of the proposed refinements to the CT-LIN contact analysis, listed above. A brief discussion of the results is presented in Section 4. Conclusions and Recommendations are presented in Sections 5 and 6, respectively.

2. RECAP OF PROGRESS TO DATE

Various CT-LIN contact assessments have been performed over the years, starting in the 1980s. This paper covers developments since 2005, when the CANDU 6 stations took a renewed interest in the topic.

2.1 CT-LIN Contact Analyses

There are three components to the prediction of CT-LIN contact: (1) Prediction of the LIN creep sag rate, (2) Prediction of the CT creep sag rate, and (3) The determination of the CT-LIN gap at a given time in-service.

Section 2.1.1 briefly covers the work on LIN creep sag. A summary of the work on the prediction of CT creep sag is presented in Section 2.1.2. Section 2.1.3 presents the work performed on determining the CT-LIN gap at given times in-service.

Section 2.1.4 presents examples of typical CT-LIN tine-to-contact predictions, illustrating changes that have been made from 2005 to 2008. The analyses performed in 2005 have been termed “First Estimate Predictions”. Further refinements subsequent to 2005 involved the updating and calibration of CDEPTH models to obtain less conservative CT creep sag rates, giving rise to “Updated “ and “Calibrated CT-LIN time-to-contact predictions”, which are explained later in the paper.

All the examples presented in this paper are from the Point Lepreau Generating Station (PLGS) or from Gentilly-2 (G-2),

2.1.1 LIN Creep Sag Modelling

Starting in about 2000, optical CT-LIN gap measurements were introduced into the strategy for dealing with potential CT-LIN contact. Since CT-LIN gap measurements were available in 2005 for PLGS and G-2, it was decided that the measurements would form the basis for calculating LIN sag rates, rather than using analytical methods. The CT-LIN gap measurements were performed at critical gaps in the reactor core. A main strategy was to measure the gap for a fuel channel that was inspected in the same outage. This would allow gap and PT sag measurements to be combined, as outlined below. The following method for determining the creep sag of the LIN (the in-service elastic curve) and the creep sag rate, was used:

1. Predict the initial elastic curve for the LIN using ANSYS 9.0
2. Using PT sag measurements for a channel directly above a LIN, calculate the elevation at the bottom of the CT at the intersection of the CT with the LIN – ideally for more than one CT, Note that elevation denotes distance below the centerline of a straight LIN
3. Add the CT-LIN gap measurement to the elevation points at the bottom of the CT to obtain points on the in-service elastic curve of the LIN (which includes creep sag).
4. Use the points on the in-service elastic curve of the LIN from 3. to generate an empirical in-service elastic curve for the LIN
5. Use in-service creep sag profiles of the CTs above the LIN and the empirical in-service elastic curve of the LIN to find the distribution of CT-LIN gaps over the length of the LIN
6. To determine the creep sag rate at any point of the LIN, subtract the in-service elevation in the empirical in-service elastic curve from the elevation in the initial elastic curve and divide by the time in service when the CT LIN gap and PT sag measurements were performed.

Figure 1 illustrates the use of LIN elevation measurements to derive in-service elastic curves for the LIN. Note that elastic curves for different end conditions of the LIN are depicted.

2.1.2 CT Creep Sag Modelling

For the predictions of CT creep sag, the CDEPTH fuel channel deformation code was the clear and obvious choice. The results shown in this paper were produced using CDEPTH 8.2.

For the time-to-contact predictions, the CDEPTH code was executed to generate fuel channel sag computations at discrete points in time, to the end of fuel channel life. The CDEPTH runs were performed for the Row F and the Row Q channels, which could contact LIN #2 and LIN #5, respectively. .

For each CT analysed with CDEPTH, the elevations at the intersection point of the CT with the LIN below it, were extracted from the CDEPTH output.

A typical plot of predicted CT elevation versus time in-service is presented in Figure 2. The CT elevation is specifically at the bottom of the CT at the intersection point of Fuel Channel Q07 with LIN #5 (denoted as Q07-L5) in PLGS.

Figure 1 – Determination of the In-Service Elastic Curve for Lin #5 in PLGS at 157 kEFPH

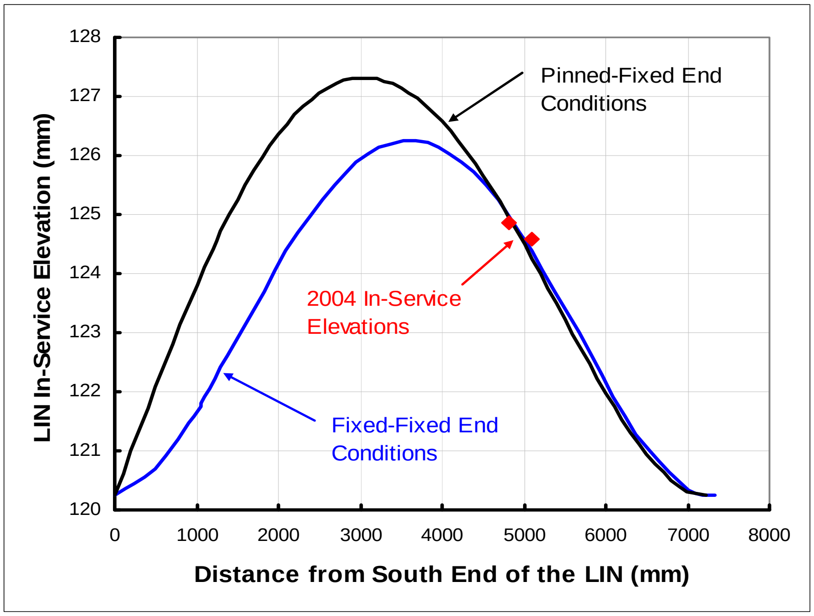

Figure 2 – Predicted Elevation of Q07-L5 Versus Time In Service With the Standard CDEPTH Fuel Channel Model

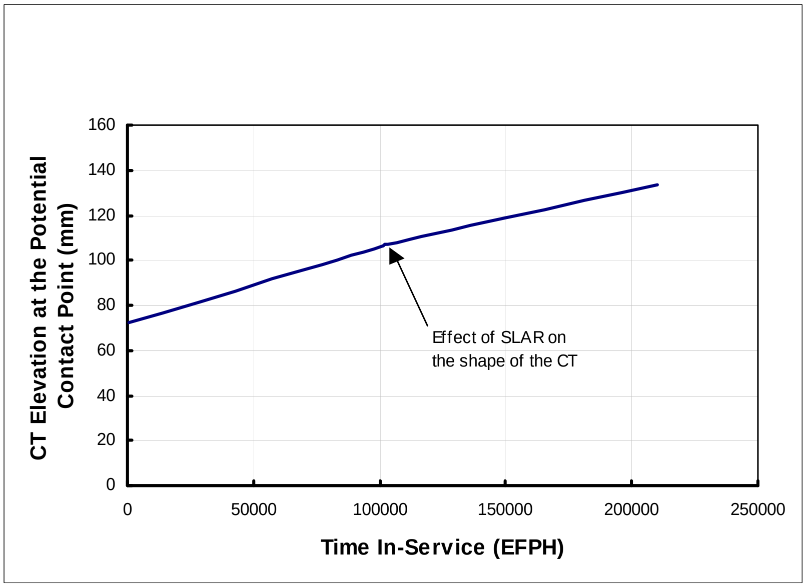

It should be noted that in the CDEPTH code, creep sag of the CT depends upon fast neutron flux, temperature, and stress. In the formulation of the input files for CDEPTH, constant lifetime average values are used for flux and temperature and stresses are calculated using initial PT and

CT dimensions. Therefore, CT creep sag rates in CDEPTH are inherently linear with time in-service.

The general feeling regarding the results in Figure 2 was that there were several sources of conservatism in the fuel channel.creep sag predictions.

Figure 3 illustrates the conservatism in the CDEPTH PT sag predictions resulting from the CDEPTH models used to generate the results in Figure 2. Figure 3 provides a comparison of measured and predicted PT sag for G-2. The data points in Figure 3 present MP ratio versus predicted sag for the inspected PTs in G-2. MP ratio denotes the ratio of Measured PT sag to the Predicted PT sag. The general trend is for MP ratio to start off around 1 early in the operating life of the reactor and then to decline with time in service. Figure 3 implies that on average, a PT with a predicted maximum creep sag of 55 mm is expected to have an actual maximum creep sag that is 18 % lower.

Figure 3 – MP Ratio for PT Sag vs Predicted PT Sag for G-2

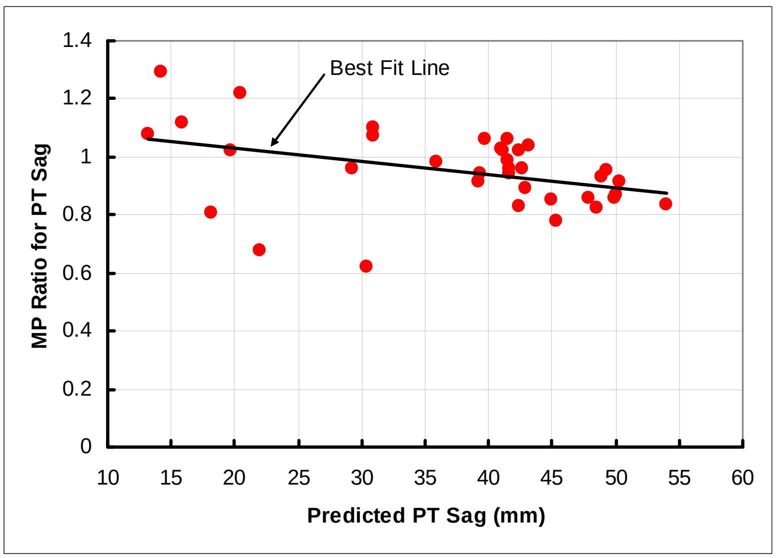

Besides the PT sag measurements, in 2004, during a fuel channel inspection in PLGS, it was found that the defueling of FC F06 resulted in a spring back of the CT of 4.5 mm, measured near the centre of the FC at the intersection point of F06 with LIN 2. The standard CDEPTH model for F06 at the time predicted a spring back of 8.4 mm due to defueling. Therefore, the overall elastic stiffness of the CDEPTH model for F06 in PLGS was found to underestimate that of the actual FC and was expected to be complicit in the over estimation of PT sag versus in-service.

2.1.2.1 Refinement to CT Creep Sag Modelling – Updated and Calibrated CDEPTH Models

Because of the findings shown in Figure 3, various modifications to the CDEPTH input models for the PT and the CT were investigated, which are outlined in Reference [1]. The purpose of the modifications was to introduce justifiable changes in the CDEPTH models to reduce conservatism in the prediction of PT sag. The modifications to the standard CCEPTH model involved:

1. PT In-Service Dimensions and CT End Bell Modelling
2. PT End Support Conditions

3. CT Ovality at Spacer Locations
4. The CT East End Support Condition

The modified CDEPTH model was termed the updated model to signify that the standard model was updated to reflect the current properties of the fuel channel.

An example of the results of updating the CDEPTH models is shown in Figure 4, in which predicted deflections of a point at the bottom of the CT in PLGS, due to elastic and creep sag, are plotted versus time in service. The standard CDEPTH model predictions are plotted in the line at the top, and the lower line represents the predictions of the updated CDEPTH model. The single data point represents the expected elevation of the CT, based on PT sag measurements

Figure 4 – Predicted CT Deflections for PLGS F06 Using Standard and Updated CDEPTH 8.2 Models

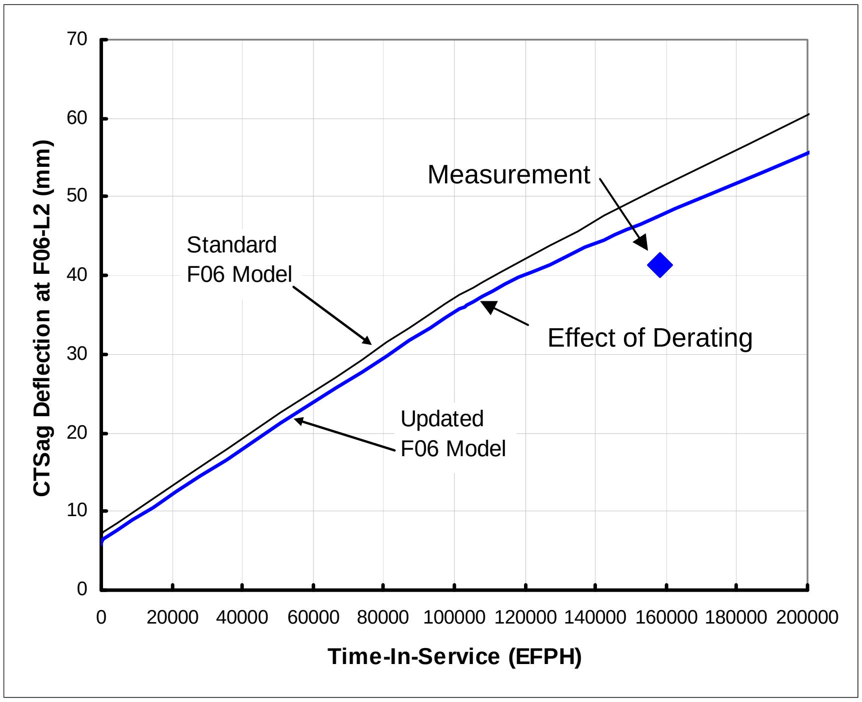

Figure 4 shows that the updated model reduces some of the conservatism in the predictions of the standard model but considerable conservatism remains, considering the position of the single measurement in the plot relative of the opdated F06 model..

A second approach involved simply calibrating the CT creep sag predictions based on MP ratio, the results of which are shown in Figure 5. In the figure, predicted elevations at Q06-L5 for G-2 from the standard and the calibrated CDEPTH models are plotted versus time in service. Also plotted as the single data point is the elevation of Q06-L5, based on PT sag measurements. Figure 5 shows that the creep sag of the CT with the calibrated model is significantly lower than that predicted with the standard model and agrees well the CT elevation expected from the PT sag measurement.

A similar approach for reducing the creep sag rates predicted with CDEPTH was used by AECL in 2010 in an analysis of Bruce Units 3 and 4. In that assessment, one of the creep constants in the CRNL 4003 deformation equation was modified to reduce the rate of creep sag for the fuel channels. The modified predictions matched measurements fairly well, but the modified CDEPTH creep sag predictions were still linear with time in service.

2.1.3 Determination of CT-LIN Gaps.

For the assessments described so far, CT-LIN gap measurements were performed by AECL using an optical camera system, as described in Reference [2]. To measure the gap, the camera was inserted into the calandria via one of the calandria view ports and the camera was positioned to record an image of the gap to be measured. The measurements involved scaling the image of the CT-LIN gap against images of the LIN or CT, which are of known dimensions

Figure 5 – Predicted CT Elevations for G-2 Q06 With Standard and Calibrated CDEPTH Models

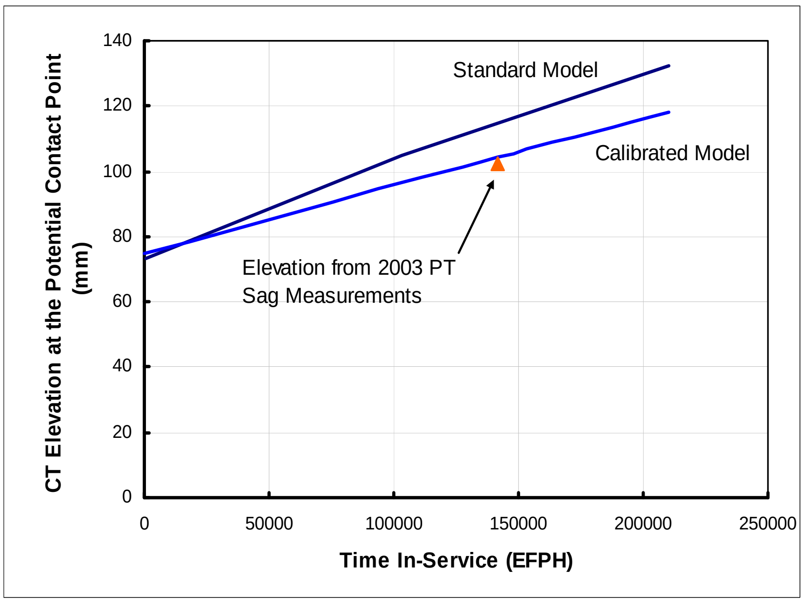

.Figure 6 displays examples of the gap measurements that were obtained in three inspections in PLGS and in G-2. The inspections in PLGS were performed in 2004 and the G-2 inspections were performed in 2003 and were repeated in 2006. The gaps plotted in Figure 6 are between the Row Q CTs and LIN #5.

Figure 6 – Example of CT-LIN Gap Measurements in PLGS AND IN G-2

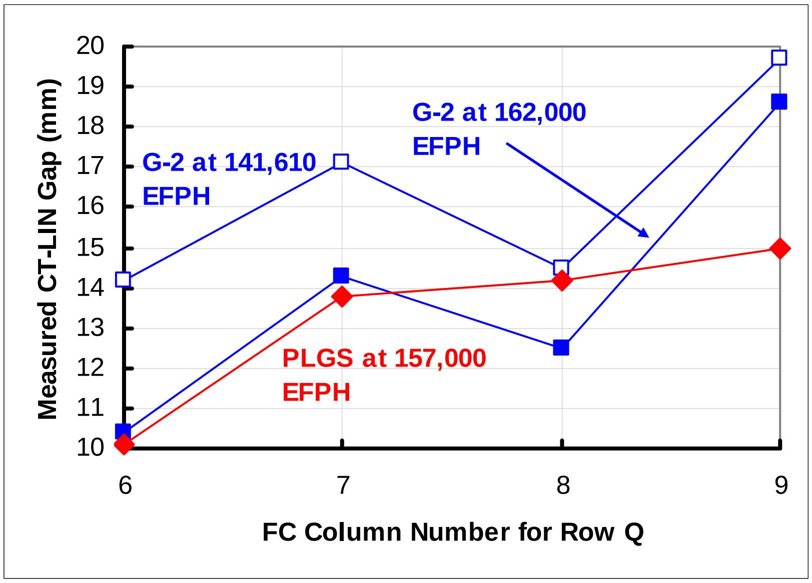

In the figure, the gap measurements are for Q06 – Q08, which could contact LIN #5.

2.1.4 CT-LIN Time-to-Contact Predictions

2.1.4.1 First Estimate Predictions of CT-LIN Time-to-Contact

These predictions were generated using CDEPTH 8.2 to model CT sag versus time in-service, while CT-LIN gap measurements were used to deduce both the rate of LIN creep sag and the initial gap between the CT and the LIN.

Time-to-contact predictions generated in this manner for Point Lepreau are presented as an example in Figure 7. The first estimate predictions indicate a number of channels with CT-LIN contact earlier than 185 kEFPH, the planned time for shutdown of the reactor for refurbishment for Q07, which was unacceptable. The earliest time-to-contact was predicted to be 181 kEFPH.

Figure 7 – Example of First Estimate CT-LIN Time-to Contact Predictions For Contact of Row Q CTs with LIN #5 in PLGS - 2005

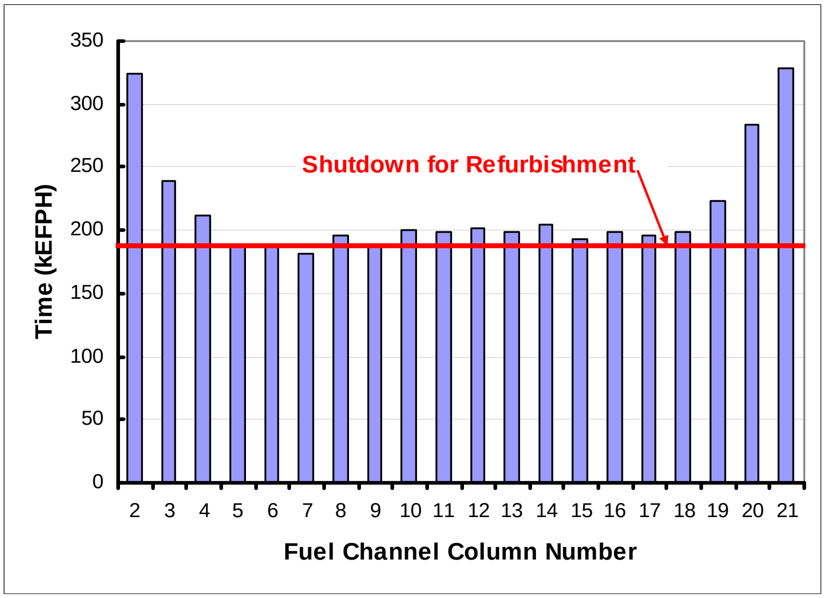

2.1.4.2 Calibrated Predictions of CT-LIN Time-to-Contact

In order to improve upon the results in Figure 7, the time-to-contact predictions were repeated using the updated and calibrated CDEPTH models. The time-to-contact predictions with the calibrated CDEPTH models are presented in Figure 8, which were considered to be acceptable. With the calibrated CDEPTH models, the earliest time-to-contact was predicted to be 210 kEFPH, an improvement of 29 kEFPH over the results in Figure 7.

Figure 8 – Time-to-Contact Predictions for the PLGS Row Q Fuel Channels Using Calibrated Fuel Channel Models With Different LIN Creep Sag Rates

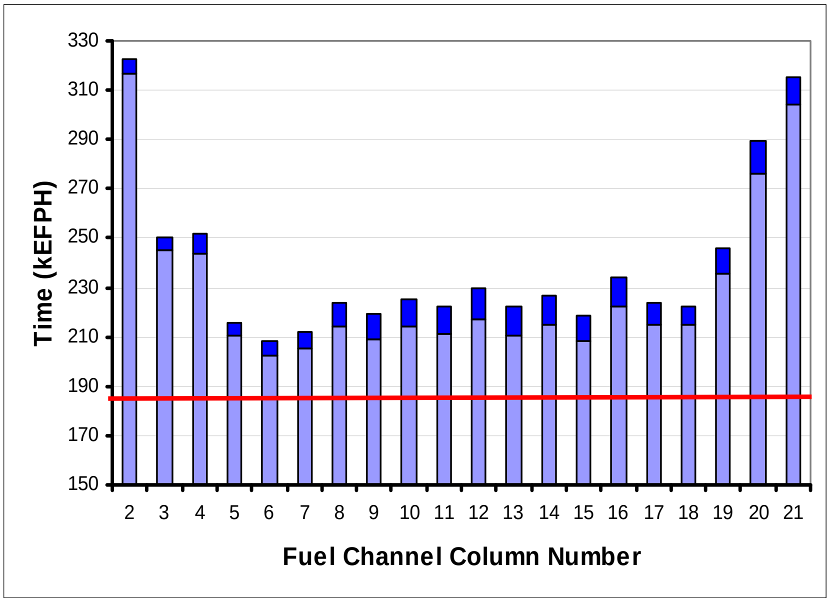

Note: the light bars represent time-to-contact for zero creep sag of the LIN beyond 157 kEFPH. The dark bars represent the increase in time-to-contact for creep sag of the LIN at the estimated rate. The total height of the light and dark bars represents the time-to-contact for creep sag of the LIN at the estimated rate. The horizontal line represents the planned time in-service for plant shutdown for retubing.

3. FURTHER REFINEMENTS TO CT-LIN CONTACT ANALYSIS

The sections that follow describe further advancements that have been made which will have an impact upon the accuracy of CT-LIN contact predictions.

3.1 APPARENT NON-LINEARITY IN PT CREEP SAG WITH TIME IN-SERVICE

From a theoretical perspective, it is expected that the creep sag rate of the fuel channel should **not** be constant but should decrease with time in service. Figure 9 presents a plot of maximum PT sag, (roughly at the centerline of the reactor) versus time in service for PLGS and for G-2.. The data covers all the PT sag measurements in the two reactors. The PLGS data are plotted in Figure 9 in red. The red line is a power function regression for PT sag versus time in-service for PLGS. Similarly, the G-2 data and power function regression a shown in blue in Figure 9.

Figure 9 – PT Maximum Sag Data with Regression Lines for PLGS and G-2.

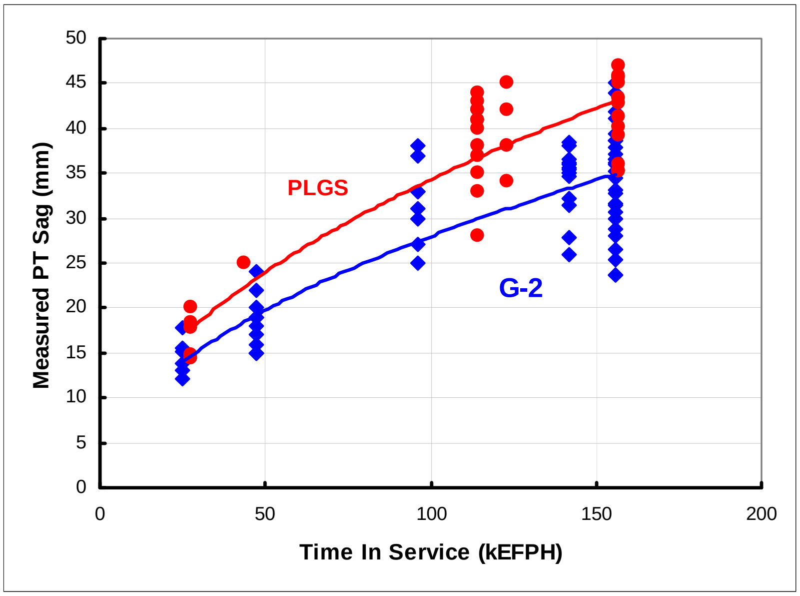

The hypothesis suggested by Figure 9 is that PT creep sag is non-linear with time in service and because of the scatter in the measurements, is multivariable. In this case, the missing variable would be fast neutron flux, based on irradiation-induced deformation theory. The measurements in Figure 9 are reminiscent of various plots that have been made of PT diametral expansion versus time in-service, which in 2005 – 2007 led to the development of multivariable regression models for PT diametral expansion for the PLGS and the G-2 PTs, issued in [3] and [4]. With the multivariable regression modeling for PT diametral expansion as a precedent, a similar analysis was tried for the PT sag data of Figure 9, the results of which are presented in Figure 10.

Figure 10 is a surface fit plot for G-2 PT sag versus time in service and FC power, noting that FC power is proportional to fast neutron flux and temperature and was chosen as a proxy for fast neutron flux

Figure 10 - Multivariable Regression Analysis for PT Sag versus Time In Service and Fuel Channel Power

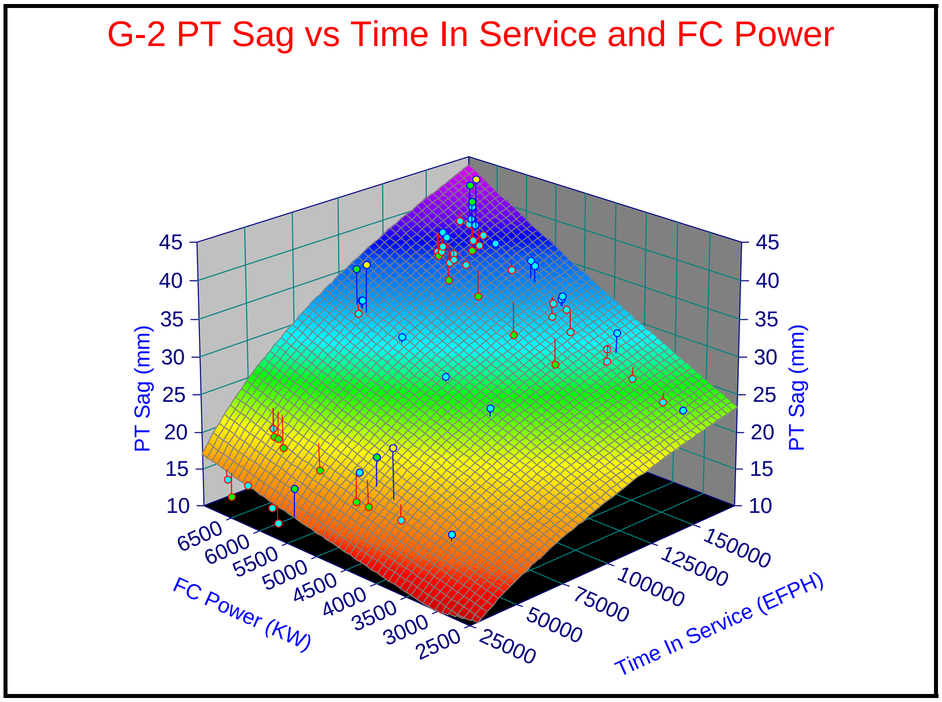

Figure 10 illustrates that the PT sag data is suitable for being fit to a non-linear multivariable model for sag versus time in-service and fuel channel power (or fast neutron flux). As an example, the surface fit depicted in Figure 10 is of the form:

$$\text{Ln (PT Sag)} = A + B/\ln(\text{Time}) + C\,(\text{FC Power})^{0.5}\ \ln(\text{FC Power})$$

Where A, B, and C are constants.

The implications of the non-linear behaviour of PT sag versus time in service for CDEPTH predictions of PT and CT sag are illustrated in Figure 3. The general trend is for MP ratio to start off around 1 early in the operating life of the reactor and then to decline with time in service. This trend is consistent with the non-linearity in PT sag observed in Figure 9. The linear sag deformation model in CDEPTH is quite representative of the PT sag measurements early in the life of the reactor, but with increasing time in service, the PT sag measurements deviate from a linear trend, causing decreases in MP ratio.

3.1.1 Rationale for the Apparent Non-Linearity in PT Creep Sag

When indications of non-linear creep sag of the PTs appeared, a physical explanation was sought for why the creep sag of the PT would decrease with time in-service, which led to the investigations summarized in this section.

In CDEPTH, the elements of the PT and CT models are modelled as straight beams, conventionally with a uniform cross-section. Intuitively, because the deformations of the PT and CT seem to be relatively small, the use of straight beam models for the PT and CT has continued in CDEPTH without any concern. However, in recent years, fairly significant PT and CT deformations have been detected. Early speculation was that the diametral deformation of the

CT and curvature of the CT would increase its stiffness and would reduce the rate of creep sag with time in-service, explaining the trend seen in Figure 9.

An investigation of the effects of PT deformation on the PT was carried out, from which it was found that seemingly small diametral expansions, combined with changes in curvature, resulting from PT sag, would influence the axial stress distribution in the PT, compared to that of a pristine PT. Similarly, small deformations of the CT would alter the stress distribution in the CT, compared to that in a pristine CT.

An example of the effect of CT curvature, due to creep sag, combined with local deformation of the CT cross-sections on the distribution of axial stress due to bending of the CT, is presented below. The example is for the CT of Fuel Channel F06 in PLGS, which was inspected in 2004 at 157 kEFPH.

From the inspection of F06, in 2004, PT sag and curvature measurements were obtained. The sag and curvature profiles aee given in Figure 11. In addition, PT gauging data were combined with PT-CT gap profiles to generate estimated CT inner diameter profiles, depicted in Figure 12. The profiles feature local diametral expansion of the CT at spacer locations. The expansions are in the vertical direction only, and induce ovality in the CT, such that at the spacer location, the vertical diameter of the CT exceeds the horizontal diameter. Both curvature due to sag and CT diametral expansion were thought to stiffen the CT.

Figure 11 – PT Sag and Curvature for PLGS F06 at 157 kEFPH

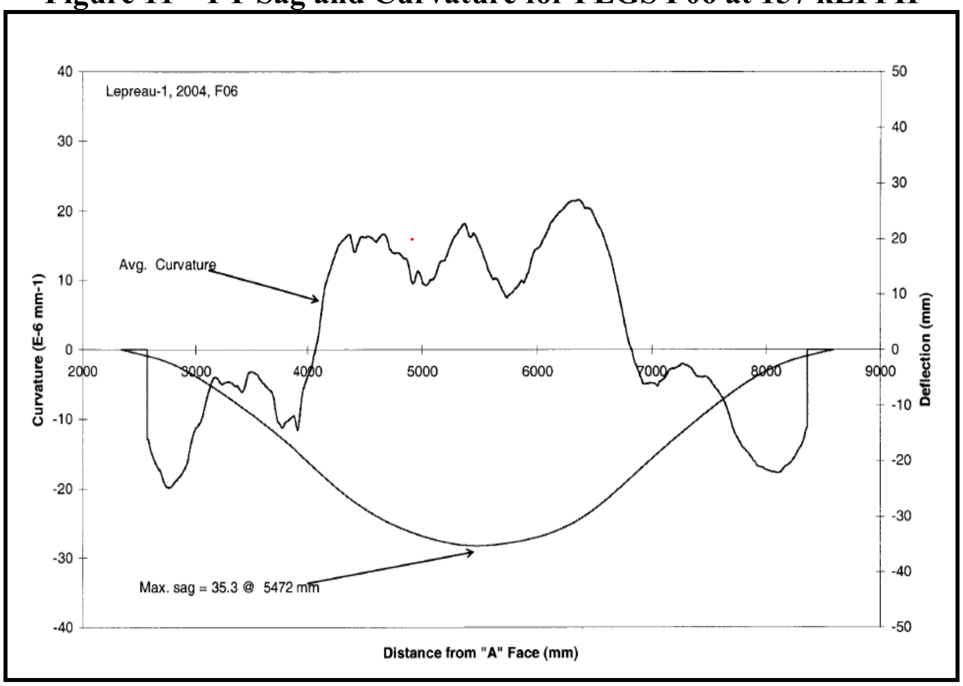

Figure from 87-31100-PIP-003, provided by T. Langlais, NB Power Nuclear

Figure 12 -Inner Diameter Profiles for the CT of F06 in PLGS at 157 kEFPH

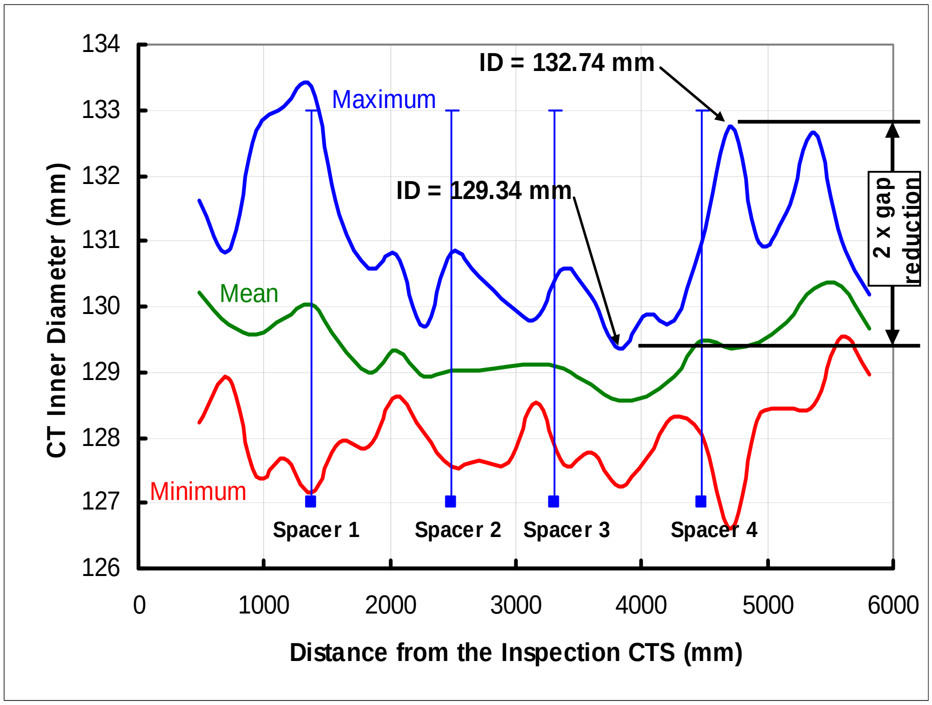

CTS stands for calandria tube sheet. The nominal inside diameter of the CT is 129 mm. At various sections of the CT, deformation has altered the section properties of the CT. The stress distribution at these sections deviates from that for a circular CT.

Following that line of thought, a comparative stress analysis was performed for the pristine CT in F06 and for the deformed CT at 157 kEFPH. . The pristine CT was assumed to be straight and cylindrical, which is how the stresses in the CT are calculated in CDEPTH. The deformed CT was assigned local curvatures due to creep sag and vertical and horizontal outer diameters based on the results of the inspection at 157 kEFPH, shown in Figures 11 and 12.

For both cases, . $\boldsymbol{\sigma}$/M was calculated for sections of the CT at discrete axial positions along the length of the CT, where $\boldsymbol{\sigma}$ is the axial stress due to bending and M.is the applied bending moment. For the pristine CT, $\boldsymbol{\sigma}$/M was calculated using the flexure formula for straight beams.

For the deformed CT, $\boldsymbol{\sigma}$/M was calculated using the following closed form solution for beams of constant curvature:

$$\sigma = \frac{My}{Ae(R-y)}$$

Where y is the distance from the neutral axis for the given section, A is the cross-sectional area of the section of the CT, e is the eccentricity of the section (the distance between the neutral axis and the geometric centroid of the section, and R is radius of curvature for the section.

The results of the comparative stress analysis are presented in Figures 13 and 14. In Figure 13, σ/M values at the top and bottom of the pristine and the deformed CT, at a section near the centre of the CT, are plotted versus distance from the neutral axis.

Based on Figure 11, the maximum axial stress in the deformed CT of Fuel Channel F06 near the central plane due to bending of the CT is 0.4 times the corresponding stress in the straight CT. Since the radius of curvature if the deformed CT is considered to be very large, the results in Figure 13 were surprising.

Figure 13 – Plot of Axial Stress due to Bending for the Pristine and the Deformed CT of F06 at 157 kEFPH at a Central Section

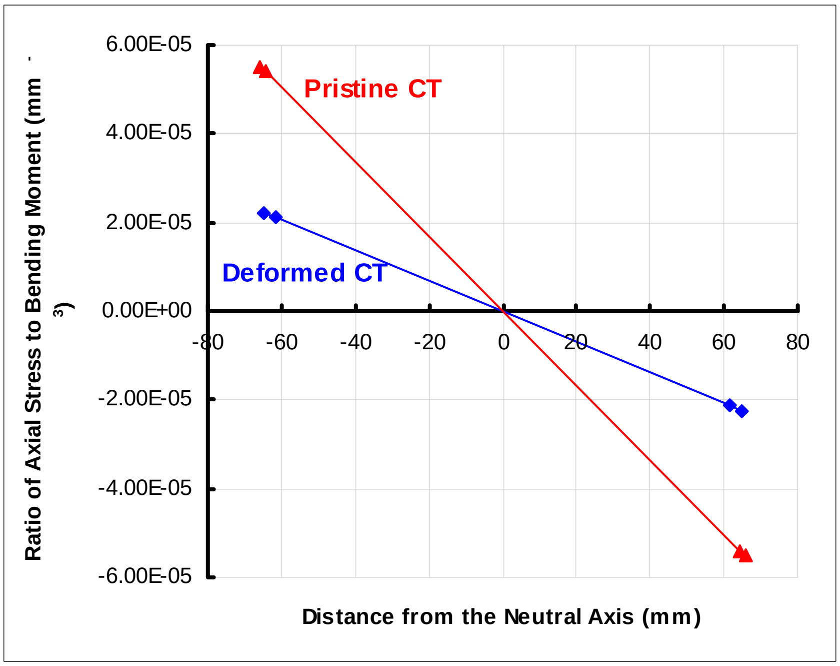

In Figure 14, the ratio of maximum σ/M value for the deformed CT to that for the pristine CT is plotted for various sections of the CT. Over most of the length of the CT, the ratio approaches 0.4, as can be seen in the Figure.

The reduction in bending stress in the deformed CT is due to a combination of the curvature of the CT and an increase on the cross-sectional area of the CT because of diametral expansion of the CT.

Figure 14 – Plot of Bending Stress Ratio for the Deformed and Pristine CT from F06 in PLGS versus Distance from the Outlet EF Taper

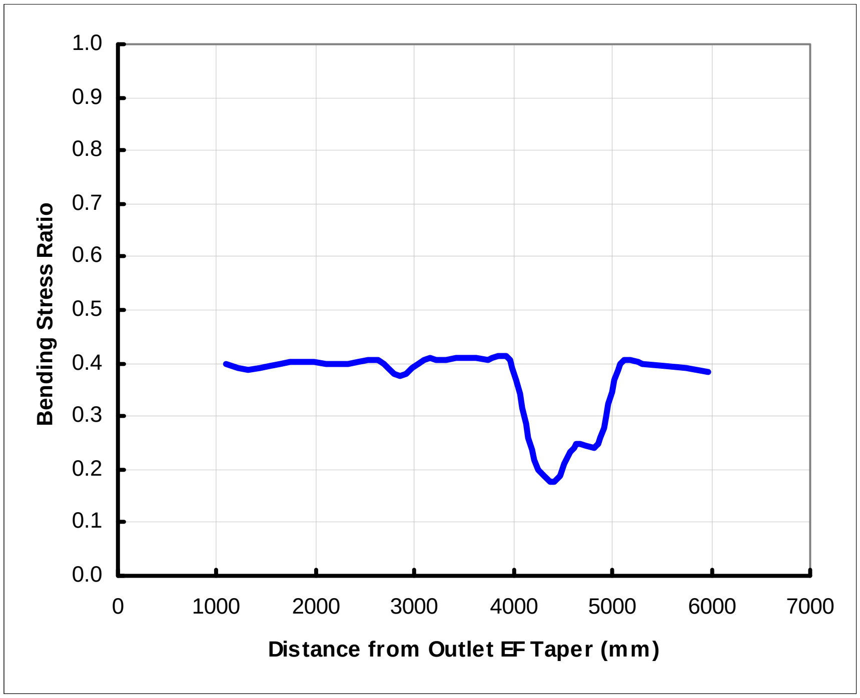

Note: EF stands for End Fitting. CT diameter data was questionable from 0 – 1000 mm and so the stress ratio was not plotted for this range. The local depression in the stress ratio from 4000 – 5000 mm coincides with a region of higher curvature and increased ovality of the CT due tospacer loading.

Since bending stress drives creep sag of the CT, for a bending stress at 157 kEFPH in the deformed CT that is 0.4 of the stress for a pristine CT, the CT creep sag rate at 157 kEFPH should be 0.4 of the initial creep sag rate, if all other parameters that affect CT sag were constant.

The possible relationship between CT creep sag rate and the reduction in bending stress in the deformed CT was investigated in Figure 15. In the figure, PT creep sag rate, determined from the PT sag data for PLGS of Figure 9, was plotted versus time in-service, together with a best-fit line and a trend line for F06, depicted in red. From Figure 15, the mean initial creep sag rate and the mean creep sag rate at 157 k EFPH were found to be 4.2 and 1.8 mm per 7 kEFPH. On average, over all inspected PTs, the creep sag rate at 157 kEFPH was found to be 0.43 of the initial sag rate, measured at 27 kEFPH.

Similarly, from the trend line for F06 drawn in Figure 13, the final PT creep sag rate at 157 kEFPH was found to be 0.39 times the initial PT creep sag rate for F06.

In summary, assuming that the CT creep sag rate for F06 is proportional to the PT creep sag rate, the predicted bending stress reduction in the CT of (100 – 40)% = 60% from 27 to 157 kEFPH was accompanied by a CT creep sag rate reduction of (100 – 39)% = 61%.

Note that the stress reduction numbers quoted above assume that there were no changes in bending moment at the central section of the CT from 27 to 157 kEFPH. In reality, complications such as SLAR and the redistribution of spacer loading could alter the bending moment distribution acting on the CT. These effects could introduce secondary changes to the bending stress in the CT. Therefore, the actual bending stress in the CT of F06 at 157 kEFPH could deviate from 0.40 of the stress for an undeformed CT.

Another point to consider in comparing the predicted stress reduction in the CT to the creep sag rate of the PT is that there will be small differences in the sag rate of the PT and CT between the spacers. Therefore, except for the spacer locations, using the PT sag rate as the CT sag rate will overestimate the sag rate of the CT

Setting aside, temporarily, the complications that could have changed the bending moments acting on the CT of F06 during operation to 157 kEFPH, the implication is that stress reductions in the CT due to CT deformation could be responsible for 60/61 = 98% of the reduction in creep sag rate for F06 from 27 to 157 kEFPH.

Figure 15 – PT Creep Sag Rates Versus Time In Service for PLGS

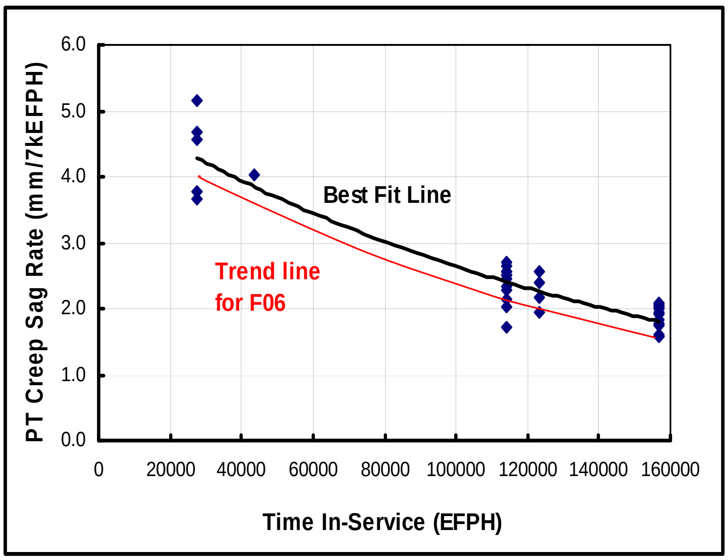

3.2 LIN CREEP SAG BEHAVIOUR

The original approach for establishing the in-service elastic curve of the LIN was to use the elevation of the deformed PT plus the PT gap to calculate the in-service elevation of the LIN at its intersection point with the fuel channel. This strategy was abandoned when discrepancies in some of the CT-LIN gap measurements came to light, as outlined in 3.3.

Later, it was found that ultrasonic measurements of LIN elevation in Wolsong, reported in Reference [5] produced in-service sag profiles that agreed very well with predictions generated with the NOZZLE code. Figure 16 provides a plot of the initial and in-service elastic curves at 1.8 and at 18 years in service for the Wolsong reactors, based on NOZZLE predictions. The data points shown in red in Figure 16 represent measurements [6}.

For CANDU 6 reactors, LIN creep sag can be calculated using the data of Figure 16. For other reactors, the NOZZLE code should give very good results.

FIGURE 16 – Comparison of Sag Measurements with Sag Profiles from the NOZZLE Code for the Wolsong Reactors

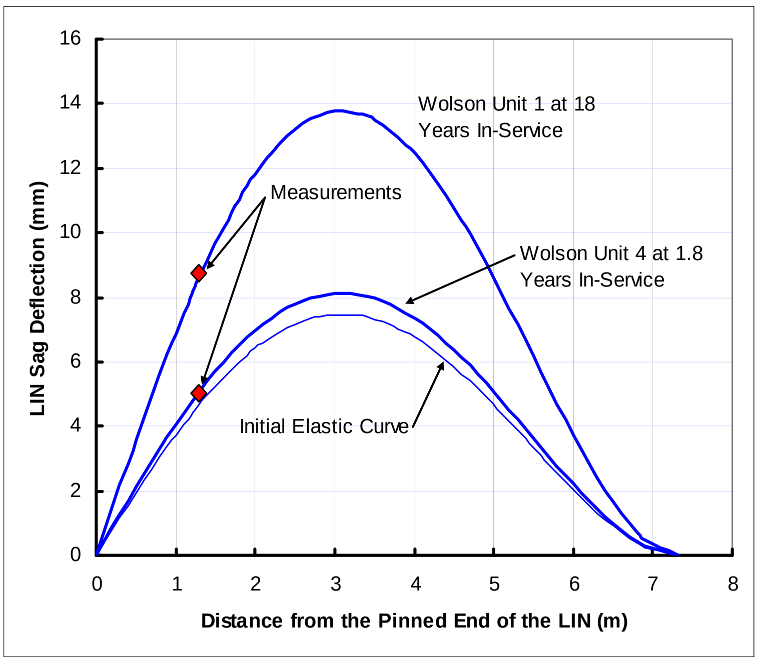

3.3 CT-LIN GAP MEASUREMENTS

Following an examination of the optical CT-LIN gap measurements for G-2, it appeared that some of the gaps were underestimated by about 10 mm, based on the known elevation of the fuel channel and as-installed elevation . The accuracy of the gap measurements was investigated at length but an explanation for the apparent discrepancies was not found.

Recently, two factors have been identified as causes for the underestimation of gap sizes using the optical method of gap measurement: (1) Sag of the LIN, and (2) elevation of the camera relative to gap being imaged.

Figure 17 illustrates how the image of the CT- LIN captured by the camera can underestimate the size of the actual gap as a result of LIN sag. The image of the gap is formed by light passing between the CT and the LIN. In this case, the camera is at the same elevation as the space between the CT and the LIN that forms the gap image. The height of the beam of light passing between the CT and the LIN is determined by the vertical distance between the bottom of the CT and the highest point at the top of the LIN along its length. As shown in the figure, the bottom of the CT and the highest point at the top of the LIN are not equidistant to the camera because of the sag of the LIN. Because of the sag of the LIN, as depicted in the figure, the actual gap is larger than the image of the gap, captured by the camera.

To avoid the effect of LIN sag on gap image, gap imaging must be performed with the camera perpendicular to the LIN. With the arrangement of view ports in the calandria, only a few of the gap images can be generated with the camera perpendicular to the LIN.

Figure 17 – Underestimation of Gap Size due to Sag of the LIN

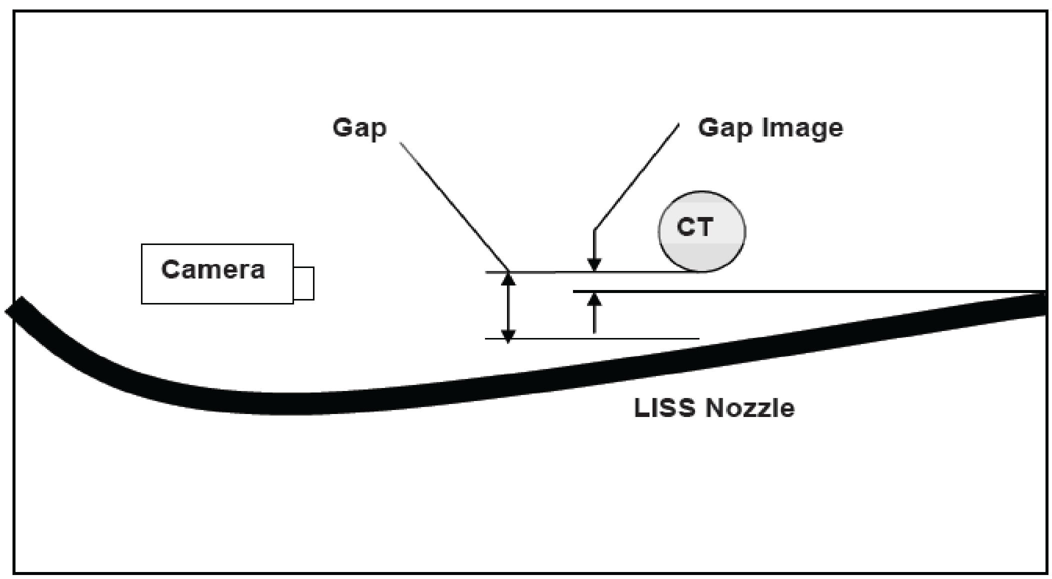

Figure 18 illustrates how elevation of the camera relative to the gap reduces the size of the gap image that is captured by the camera. In this example, the LIN is assumed to be straight and the camera is inclined at an angle θ relative to the LIN. At θ = 0º, the camera would be at the same height as the top of the LIN and the gap image would be a good representation of the actual gap size. However, with increases in θ, as depicted in Figure 5, the apparent space between the CT and LIN would decrease, reducing the size of the gap image.

It is expected that the inclination of the camera is not strictly controlled during the gap measurements.

Figure 18 – Underestimation of Gap Size due to Elevation of the Camera Relative to the CT

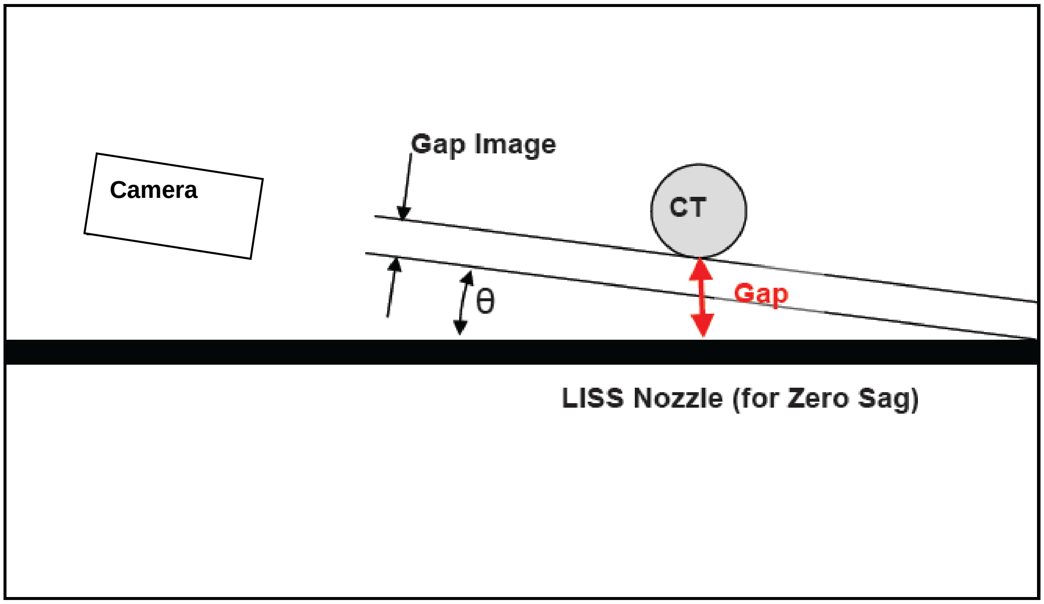

4. DISCUSSION

The comparative stress analysis of the deformed and pristine CT in F06 produced a stress ratio that was very close to the observed reduction in PT creep sag rate for F06, which was very encouraging. However, the analysis was overly simplistic. A number of variables were excluded from the stress analysis, such as changes in bending moment due to evolution in spacer load and SLAR and differences in the creep sag rate of the PT and the CT. It is expected that the stress ratio will change somewhat if a more elaborate stress analysis were performed. This means that in order to take credit for the effects of stress reductions in the CT, far more detailed finite element stress analyses of the CT should be conducted that account for the actual 3D shape of the CT, with realistic time-dependent spacer loads, including simulations of SLAR.

Regarding the creep sag behaviour of the LIN, it is noteworthy that the NOZZLE code, from 1981, generated initial elastic curves and creep sag prediction that agree well with the ultrasonic LIN sag measurements in Wolsong, issued in 2005.

5. CONCLUSIONS

1. PT sag measurements from the inspection of PLGS and G-2 indicate that PT, and therefore CT creep sag, are non-linear functions of time in service.

2. Based on a simple comparative stress analysis of a pristine and a deformed CT, deformation of the CT (creep sag and diametral expansion) will reduce bending stresses in the CT.

3. In the case of F06 in PLGS, it was found that the predicted percentage bending stress reduction due to the measured deformation of the CT at 157 kEFPH, corresponded very closely to the observed percentage reduction in PT creep sag rate from 27 to 157 kEFPH. This result implies that the reduction in bending stress associated with the deformation of the CT causes a proportionate reduction in the creep sag rate of the CT with time in service.

4. For the optical CT-LIN gap measurements, reasonable accuracy in the measurement can only be achieved if the camera is in close proximity to the gap being recorded.

5. The predictions of LIN creep sag behaviour from the NOZZLE code [5], agree closely with ultrasonic measurements of LIN elevation performed in Wolsong Units 1 and 4 [6].

6. RECOMMENDATIONS

1. In the absence of reactor-specific CT-LIN gap or LIN sag measurements, LIN creep sag predictions should be performed with the NOZZLE code or an equivalent formulation.

2. Future predictions of CT-LIN time-to-contact should take advantage of the observed non-linearity in the rate of fuel channel creep sag with time in service. To do this, CDEPTH or whichever code is used to predict PT and CT deformation, should be modified to calculate operating stresses that account for ovality and curvature of the PT and the CT, which will increase with time in service. This modification should be supported by a detailed finite element study of the in service stresses of as many inspected fuel channels as possible.

3. In future CT-LIN gap measurements, the optical camera system should only be used if the camera can be positioned at the gap to be recorded. If not, then an alternative method should be implemented.

7. REFERENCES

1. P.J. Sedran, CPUS Limited, *CT-LIN Time-to-Contact Predictions for PLGS using Updated FC Models*, CPUS Technical Report 0040 REPT ENG 0003 00, September 30, 2005

2. T. Campbell, *AECL Inspection Report Calandria Tube to LISS Nozzle Gap Measurement*, 87-31230-INR-001 Revision 1, January 2005.
3. E. Nadeau, W. Hartmann, AECL Technical Document 87-31100-220-054, *Diametral Expansion Assessment of Gentilly-2 and and Point Lepreau NGS –*

Interim Results , 2005 05.

4. P.J. Sedran, CPUS Limited, *Multi-Variable Regression Analysis of Diametral Expansion for the PLGS Pressure Tubes*, 0065-REPT-ENG-003 Rev. 00, April 27, 2007.
5. A.R. Causey and J.D. Brown, *Deflection of Liquid Poison Injection Nozzles Resulting from Irradiation-Induced Creep and Growth*, CRNL □ 2145, November 1981.
6. T.R. Kim, S.M. Sohn, J.S. Lee, Korea Electric Power Research Institute, *Ultrasonic Devise to Measure Gap Between Calandria Tube and LISS Nozzle*, 7th International CANDU Maintenance Conference, Toronto, November 20 – 22, 2005.

8. ACKNOWLEDGEMENTS

Thanks are due to Bill Rankin, NB Power Nuclear, PLGS and to Michel Cantin, Hydro-Québec - Centrale Gentilly-2 for permission to use data from various inspections and for their review of the paper. Ness Azer and Majid Tabatabai of AMEC NSS are acknowledged for their contributions as well.